Incorporation of Multinuclear Copper Active Sites into Nitrogen-doped Graphene for Electrochemical Oxygen Reduction

Masaru Kato,*[,†,‡,§] Marika Muto,[‡,§] Naohiro Matsubara,[‡,§] Yohei Uemura,[∥] Yuki Wakisaka,[¶] Tsubasa Yoneuchi,[‡,§] Daiju Matsumura,[#] Tomoko Ishihara,[⊥] Takashi Tokushima,[⊥] Shin-ichiro Noro,[†,‡] Satoru Takakusagi,[¶] Kiyotaka Asakura,[¶] and Ichizo Yagi*[,†,‡,§]

[†]Faculty of Environmental Earth Science and [‡]Graduate School of Environmental Science, Hokkaido University, N10W5, Kita-ku, Sapporo 060-0810, Japan. [§]Global Research Center for Environment and Energy based on Nanomaterials Science (GREEN), National Institute for Materials Science (NIMS), Tsukuba 305-0044, Japan. [∥]Department of Materials Molecular Science, Institute for Molecular Science, Myodaiji-cho, Okazaki 444-8585, Japan. [¶]Institute for Catalysis, Hokkaido University, N21W10, Kita-ku, Sapporo 001-0021, Japan. [#]Materials Sciences Research Center, Japan Atomic Energy Agency, 1-1-1 Koto, Sayo, Hyogo 679-5165, Japan. [⊥]Soft X-ray Spectroscopy Instrumentation Unit, RIKEN Spring-8 Center, RIKEN, Sayo-cho, Sayo, Hyogo 679-5148, Japan.

Keywords: Oxygen reduction reaction; Polymer electrolyte fuel cell; Electrocatalysts; Nitrogen-doped graphene; Metalloenzymes.

Abstract

Multinuclear metal active sites are widely used as catalytic reaction centers in metalloenzymes and generally show high catalytic activity. For example, laccases are known to catalyze the oxygen reduction reaction (ORR) to water at a multinuclear copper site with almost no energy loss. The ORR is an important reaction not only in oxygenic respiration but also in future energy generation devices such as polymer electrolyte fuel cells and metal–air batteries. For large-scale commercialization of these devices, there is a need to develop highly active ORR electrocatalysts based on non-precious metals. Incorporation of multinuclear metal active sites in conductive materials such as carbon will allow us to develop highly active electrocatalysts like metalloenzymes. However, such methods had not been established yet. Herein, we report a copper-based ORR electrocatalysts with multinuclear copper active sites in nitrogen-doped graphene. The electrocatalyst was synthesized from the mixture of graphene oxide and a multinuclear copper complex in a short-period heating method.

Electrochemical measurements revealed that the obtained electrocatalyst showed the highest electrocatalytic activity for the ORR in the Cu-based electrocatalysts in neutral aqueous solution. Physicochemical measurements including *in situ* X-ray absorption spectroscopy revealed the incorporation of multinuclear copper sites. Our synthetic approach will offer guidance for developing highly active electrocatalysts utilizing multinuclear metal sites not only for the ORR but also for other electrocatalytic reactions.

1. INTRODUCTION

Oxygen reduction reaction (ORR) is a key reaction in electrochemical energy conversion devices such as polymer electrolyte fuel cells (PEFCs) and metal–air batteries.[1,2] In PEFCs, the ORR is catalyzed at the cathode and its slow kinetics limit the performance of PEFCs. In state-of-the-art PEFCs, platinum-group metal (PGM) alloys are used as electrocatalysts for the ORR. Pt is rare and expensive, and there is a need to develop non-PGM-based electrocatalysts with high catalytic activity for large-scale commercialization of PEFCs.

One of the promising synthetic approaches to non-PGM electrocatalysts for the ORR is pyrolysis of precursor mixtures containing low-cost 3d transition metal, nitrogen and carbon sources, for example, mixtures of metal salts and nitrogen-containing ligands/polymers.[3–8] Non-PGM electrocatalysts prepared in pyrolysis generally shows high catalytic active for the ORR. However, these active site structures are still under debate because heat treatments involve complicated reaction processes such as fragmentation of precursors.[3,8–10] Another promising approach is a bio-inspired approach. The ORR is a key reaction not only in PEFCs and metal-air batteries but also in oxygenic respiration. Metalloenzymes such as laccases catalyze the ORR with almost no overpotential.[11] Laccases use a multinuclear copper complex as the

catalytic reaction center and this multinuclear core structure has inspired us to synthesize functional mimics of copper-based electrocatalysts for the ORR.[12–16]

Herein, we report synthesis, characterization and electrocatalytic ORR activity of a Cu−N co-doped carbon electrocatalyst, r[Cutrz/GO]. This electrocatalyst was synthesized in pyrolysis from a multinuclear copper(II) complex (Cutrz)[17] and graphene oxide (GO), as shown in **Figure 1**. Cutrz has a nitrogen-rich ligand of 1,2,4-triazole (trz) and serves as the template for the formation of catalytic active sites. Triazole ligands are known to provide multinculear copper coordination environments suitable for the ORR.[12,15,16,18] Cutrz is easily prepared in one step and its multinuclear copper core resembles the active site of laccases. GO as the additional carbon source can be converted to reduced graphene oxide (rGO) in pyrolysis. The reduction of GO in the presence of metal and nitrogen sources involves the incorporation of metal active sites into conductive sp^2 carbon networks.[3,8,19]

2. MATERIALS AND METHODS

2.1. Materials. A 5% Nafion® 117 dispersion was purchased from Wako Pure Chemical Industries Ltd. Graphite powder (<20 microns) was commercially available from Sigma Aldrich. The trinuclear copper(II) complex, $[Cu^{II}_3(trz)_3(\mu\text{-}OH)]Cl_2\cdot 6H_2O$

(Cutrz), was prepared, according to the literature.[17] Cutrz was characterized by elemental analysis and X-ray diffraction. Ultrapure oxygen (purity, 99.9999%) and ultrapure argon (purity, >99.9995%) was used for electrochemical measurements.

2.2. Preparation of graphene oxide (GO). Graphene oxide (GO) was prepared based on a modified Hummer's method.[20,21] A mixture of graphite (1.0 g) and $NaNO_3$ (0.50 g, 5.8 mmol) in 23 mL of conc. H_2SO_4 was stirred in an ice bath, and then $KMnO_4$ (3 g, 19 mmol) was slowly added to the reaction mixture keeping the solution temperature at <20°C. The reaction mixture was stirred at 35°C for 30 min, heated under stirring at 98°C in an oil bath, followed by addition of Milli-Q water (46 mL), stirred at 98°C for 15 min, and then cooled to room temperature. Milli-Q water (140 mL) and a 30% H_2O_2 aqueous solution (1 mL) were added to the reaction mixture at room temperature, and then the mixture was kept at room temperature overnight, giving a dark-yellow precipitate of GO. The GO was separated from the supernatant by decantation, washed twice each with Milli-Q water (ca. 40°C), 30% HCl aqueous solution, EtOH and Et_2O by using a centrifuge (KUBOTA 3700 equipped with an angle rotor AF-5004CA) at 6000 rpm for 10 min, and then dried under vacuum to obtain ca. 1.7 g of GO.

2.3. Preparation of GO-supported Cutrz (Cutrz/GO). The electrocatalyst r[Cutrz/GO] was prepared in a short-period heating method.[19,22] Cutrz (0.16 g, 0.27

mmol) and GO (1.0 g) were dispersed in EtOH (10 mL). The dispersion was sonicated for 30 min and then stirred at room temperature overnight. The product was filtered and dried under vacuum at room temperature, yielding ca. 0.22 g of Cutrz/GO.

2.4 Heat treatment of Cutrz/GO for the preparation of r[Cutrz/GO]. Cutrz/GO (10 mg) was placed in a carbon pot (20 mmφ×20 mmH), heated in the reaction chamber of an electromagnetic inductive heating furnace (MU-1700D, SK MEDICAL ELECTRONICS Co., Ltd.) from room temperature to 1273 K with a ramp rate of 450 K/min under Ar, hold at 1273 K for 45 s under Ar and then naturally cooled down to room temperature in the heating chamber under Ar, giving ca. 2 mg of the as-prepared catalyst, r[Cutrz/GO]. A copper content in the as-prepared r[Cutrz/GO] was determined to be 6±3 wt% by using ICP-AES. To optimize heating conditions, we also prepared r[Cutrz/GO] at different heating temperatures of 1073 K, 1173 K, and 1373 K.

The as-prepared r[Cutrz/GO] was dispersed in 0.5 M H_2SO_4 aqueous solution, heated at 353 K for 15 min, filtered out and then dried under vacuum. A copper content of the acid-treated r[Cutrz/GO] was determined to be 0.057±0.004 wt% by using ICP-AES.

The acid-treated r[Cutrz/GO] was dispersed in a 40 mM $CuCl_2$ aqueous solution (100 mL) and the solution was stirred at room temperature overnight. The final product

was filtered and dried under vacuum. A copper content in the final r[Cutrz/GO] was determined to be 0.28±0.02% by using ICP-AES. Elemental analysis gave 92.01% for C, 0.83% for H and 1.06% for N.

2.5. Preparation of metal-free r[trz/GO]. A dispersion containing GO (0.1 g) and 1,2,4-triazole (0.0055 g, 0.080 mmol) in 10 mL of Milli-Q water was sonicated for 1 h and then stirred at room temperature overnight. The precipitate was filtered out and dried under vacuum to obtain ca. 0.089 g of trz/GO. For the preparation of r[trz/GO], trz/GO was heated at 1273 K for 45 s in the same manner for r[Cutrz/GO].

2.6. Preparation of r[trz/GO]-Cu^{2+}. The r[trz/GO] was dispersed in 40 mM $CuCl_2$ aqueous solution (100 mL) and the solution was stirred at room temperature overnight. The residue was filtered and dried under vacuum.

2.7. Preparation of nitrogen-free r[Cu/GO]. A dispersion containing GO (0.1 g) and $CuCl_2 \cdot 2H_2O$ (0.0136 g, 0.080 mmol) in 10 mL of Milli-Q water was sonicated for 1 h and then stirred at room temperature overnight. The precipitate was filtered out and dried under vacuum to obtain ca. 0.089 g of Cu/GO. Cu/GO was heated at 1273 K for 45 s. The as-prepared r[Cu/GO] was treated with 0.5 M H_2SO_4 at 353 K for 15 min, followed by a 40 mM $CuCl_2$ aqueous solution (100 mL), in the same manner for r[Cutrz/GO] to obtain r[Cu/GO].

2.8. Preparation of reduced graphene oxide (rGO). GO (40 mg) was heated at 1273 K for 45 s in the same manner for r[Cutrz/GO] to obtain ca. 7.0 mg of rGO.

2.9. Preparation of reduced graphene oxide-supported Cutrz (Cutrz/rGO). Cutrz (6.0 mg, 0.010 mmol) was suspended in ethanol and sonicated for 30 min. In the same manner, a suspension of rGO (7.0 mg) in ethanol (10 mL) was also prepared. These suspensions were mixed and stirred at room temperature overnight. Suction filtration gave 8.4 mg of Cutrz/rGO.

2.10. Electrochemistry. Potentiostats of IviumStat and CompactStat (Ivium Technologies) were used with a typical three-electrode electrochemical system for all electrochemical measurements. A Ag|AgCl electrode in a saturated KCl aqueous solution was used as the reference electrode. All potentials were converted to the reversible hydrogen electrode (RHE) using the following equation: $E_{RHE} = E_{Ag|AgCl} + 0.199 + pH \times 0.059$ and shown in V vs. RHE. Carbon or Pt electrodes were used as the counter electrode. Note that no contribution of Pt to the catalytic activity of r[Cutrz/GO] was confirmed by ORR electrochemical measurements under Pt-free conditions using a carbon counter electrode, an electrochemical cell that was washed with a mixture of nitric and sulfuric acids and then with boiling water at least three times, and a glassy carbon disk thoroughly polished with alumina and diamond.

To prepare working electrodes for electrochemical measurements, a suspension containing 5 mg of a catalyst, 250 μL of EtOH and 47.5 μL of the 5% Nafion dispersion was kept under ultrasonication for 30 min. The suspension (7 μL) was drop-cast onto a glassy carbon disk (the diameter: 5 mm), which was polished with diamond aqueous dispersion (1 μm in diameter, Maruto Instrument Co., Ltd.) and rinsed with Milli-Q water under ultrasonication before use, and then dried at room temperature.

As electrolyte solutions, a 0.1 M $HClO_4$ aqueous solution at pH 1, a 0.04 M Britton-Robinson buffered aqueous solution containing 0.1 M $NaClO_4$ at pH 7 and a sodium hydroxide aqueous solution (0.1 M) at pH 13 were used. The electrolyte solution was purged with oxygen for at least 30 min before ORR measurements. Linear sweep voltammograms (LSVs) were recorded using a rotating ring-disk electrode (RRDE) at a rotating rate of 1600 rpm and a sweep rate of 5 mV s^{-1} under oxygen. After the LSV under oxygen, the electrolyte solution was purged with Ar for at least 30 min and then LSVs were recorded under Ar. All LSVs shown were recorded in the negative-going sweep under oxygen, and the corresponding LSVs recorded under Ar were subtracted as backgrounds.

For durability tests, working electrodes of r[Cutrz/GO] were prepared as follows: drop-casting of the suspension (7 μL) containing r[Cutrz/GO], Nafion and ethanol onto

a glassy carbon disk (5 mm in diameter), followed by heating of the disk at 393 K, which is higher than a glass transition temperature of Nafion (T_g = 382 K),[23] for 1 h in a furnace in the air. Durability tests of r[Cutrz/GO] were performed under potential cycling in the potential range from +0.50 V to +0.90 V vs. RHE at a sweep rate of 100 mV s^{-1} for 8000 times in an oxygen-saturated 0.04 M Britton-Robinson buffered aqueous solution containing 0.1 M $NaClO_4$ at pH 7. A porous carbon electrode (BAS) was used as the counter electrode. A reference electrode of Ag|AgCl (sat. KCl) were used.

2.11. X-ray photoelectron (XP) spectroscopy. The XP spectra of catalysts were collected on photoelectron spectrometers of JPS-9200 (JEOL). An Al target was used as X-ray sources. The peak of C=C in the C 1s region was used as an internal standard (284.7 eV) to calibrate the binding energies of the elements.

2.12. Inductively coupled plasma atomic emission spectroscopy (ICP-AES). Amounts of copper in catalyst were determined using an ICP-AES spectrometer ICPE-9000 (Shimazu Corporation). For sample preparation, catalysts were dispersed in a concentrated HNO_3 aqueous solution, and then the dispersion was stirred at room temperature overnight. The dispersion was centrifuged, and then the supernatant was diluted with Milli-Q water to prepare sample solutions in 0.1 M HNO_3.

2.13. Powder X-ray diffraction measurements. Powder X-ray diffraction (PXRD) data were collected on an X-ray diffractometer (Ultima III, Rigaku) equipped with graphite monochromatized Cu Kα radiation (λ = 0.1540562 nm) at 40 kV and 40 mA. A scanning rate was set to 2º/min.

2.14. Specific surface area measurements. The sample of r[Cutrz/GO] was pretreated at 423 K under vacuum for 21 h before specific surface area measurements. The measurements were carried out at 77 K using Belsorp-max (BEL JAPAN, INC.). Nitrogen gas was used as the adsorptive gas.

2.15. Raman spectroscopy. A DXR Raman Microscope (Thermo SCIENTIFIC Inc.) was used for Raman spectroscopy. All Raman spectra were recorded using a laser at 532 nm with a laser power of 1 mW.

2.16. Transmission electron microscopy (TEM) and scanning transmission microscopy (STEM). TEM images were taken by using JEM-2000FX (JEOL). High-angle annular dark field (HAADF) microscopy coupled with scanning transmission electron microscopy (STEM) images were obtained on a JEOL JEM-ARM200F instrument at 80 kV. Energy-dispersive X-ray spectroscopy (EDS) was performed on a Titan G2 60-300 (FEI) instrument at 80 kV.

2.17. X-ray absorption spectroscopy (XAS). Cu L_3-edge XAS measurements were

carried out at the soft X-ray beamline BL17SU,[24,25] SPring-8, Japan. The XAS data were collected under vacuum as total fluorescent yield using a standard 100 mm^2 Si photodiode. Circular polarized X-rays were used to gain a higher photon flux and to avoid unwanted polarization effects.[26,27]

In situ electrochemical Cu *K*-edge XAS measurements were performed at the beamline BL14B1, SPring-8, Japan and the beamlines BL9C and BL12C, Photon Factory (PF), KEK, Japan. The XAS data were collected at room temperature in the fluorescent mode using a 36-element solid-state detector (SSD) at BL14B1, a 7-element silicon drift detector (SDD) at BL9C and a 19-element SSD at BL12C.

A three-electrode electrochemical flow cell was used for the *in situ* XAS measurements.[28] The Ag|AgCl (sat. KCl) reference electrode and the Pt wire counter electrode were used. An Ivium Compactstat potentiostat was used to apply bias potentials to the working electrode. All *in situ* XAS measurements were performed in a 0.04 M Britton-Robinson buffered aqueous solution containing 0.1 M $NaClO_4$ at pH 7 under nitrogen or argon.

To prepare working electrodes of r[Cutrz/GO] for *in situ* XAS experiments, the catalyst ink containing r[Cutrz/GO] (2.8 mg), ethanol (693 μL) and 5% Nafion 117 dispersion (7 μL) was sonicated for at least 2 h, and then the ink (ca. 200 μL) was

drop-cast on a gold film sputtered on a Kapton window. The resulting electrode was heated in an oven at 418 K for 5 min. Ink of Cutrz supported on a carbon black of Ketjenblack ECP300 was prepared, according to the literature.[28]

In situ XAS data were analyzed using software packages REX2000 (Rigaku Co.) or Athena (Demeter 0.9.24). Extended X-ray absorption fine structure (EXAFS) oscillation values, $\chi(k)$, in the k range from 3 Å^{-1} to 12 Å^{-1} were extracted from XAS spectra using a spline smoothing method. The $k^3\chi(k)$ values were Fourier-transformed into R-space, followed by the inverse Fourier transform into k-space for curve-fitting using the following equations.

$$k^3\chi(k) = S_0^2 \sum_j \frac{k_j^2 N_j F_j(k_j) \exp(-2k_j^2\sigma_j^2)}{r_j^2} \sin(2k_j r_j + \phi_j(k_j)) \qquad \text{Eq. 1}$$

$$k_j = (k^2 - \frac{2m\Delta E_{0j}}{\hbar^2})^{\frac{1}{2}} \qquad \text{Eq. 2}$$

S_0^2, N_j, r_j, ΔE_{0j} and σ_j indicate the amplitude reduction factor, the coordination number, the bond length, the energy difference between the calculated and experimental threshold energies, and the Debye-Waller factor for the jth coordination shell, respectively. The phase function, $\phi_j(k)$, and the amplitude function for the jth coordination shell, $F_j(k)$, were calculated using the FEFF8.20 program.[29,30] For FEFF calculations, a molecular geometry was taken from the single crystal X-ray analysis data of $[Cu^I_3(trz)_2][Cu^I_2(trz)Cl]Cl\cdot 3H_2O$.[31] The curve-fitting analysis was performed using

the REX2000 software package.[32–34]

3. RESULTS AND DISCUSSION

The r[Cutrz/GO] electrocatalyst was prepared from GO-supported Cutrz (Cutrz/GO) at 1273 K for a short period of 45 s under Ar. The use of GO as a precursor allows the period of heat treatment to be drastically shortened for graphitization.[19] The short-period heating method minimizes the formation of metal nanoparticles, desorption of doped nitrogen atoms, and possibly the fragmentation of the metal precursor during the pyrolysis. The as-prepared r[Cutrz/GO] was dispersed in 0.5 M H_2SO_4 at 80°C to remove metallic copper, which was confirmed by using powder X-ray diffraction (**Figure S1**), and then treated with an aqueous solution containing $CuCl_2$ to obtain the final product.

The r[Cutrz/GO] electrocatalyst showed the highest ORR activity in neutral solution in the synthetic Cu-based ORR electrocatalysts, revealed by linear sweep voltammograms (LSVs). Catalytic currents were observed in LSVs of r[Cutrz/GO] under O_2 (**Figure 2a**) but not under Ar (**Figure S2**), allowing us to confirm the catalytic ORR activity of r[Cutrz/GO]. An onset potential (E_{onset}) of r[Cutrz/GO] for the ORR was determined to be ca. +0.82 V *vs*. RHE, suggesting the highest ORR activity at pH 7

in the synthetic Cu-based ORR catalysts reported to date.[12,14] Low ring currents confirmed the selective ORR to water (≤ 5% H_2O_2 production, **Figure S3**). LSVs of r[Cutrz/GO] at pH 1, 7 and 13 revealed that the catalytic activity increased with increasing pH, and E_{onset} for the ORR was determined to be ca. +0.95 V *vs*. RHE at pH 13 (**Figure S3**). This E_{onset} is comparable with that of Pt/C.[35] The ORR activity of r[Cutrz/GO] depended on the heating temperature: r[Cutrz/GO] prepared at 1273 K showed higher ORR activity than those at 1073, 1173 and 1373 K (**Figure S4**). Thus, the r[Cutrz/GO] prepared at 1273 K was used for further studies.

Control experiments confirmed that Cutrz worked as the template for the formation of highly active catalytic sites for r[Cutrz/GO]. The E_{onset} of r[Cutrz/GO] is clearly more positive than that of the precursor mixture of Cutrz/GO (**Figure 2a**), indicating that the heat treatment is crucial for the formation of the highly active reaction center. The rGO-supported Cutrz is less active than r[Cutrz/GO] (**Figure 2a**), suggesting that the immobilization of Cutrz on conductive carbon is insufficient to give the highly active catalytic site. The E_{onset} of r[Cutrz/GO] is also more positive than those of the other control samples (**Figure 2a**): the Cu-doped (N-free) graphene (r[Cu/GO]), the N-doped (Cu-free) graphene (r[trz/GO]) and the r[trz/GO] that was treated with an aqueous solution containing Cu^{2+} (r[trz/GO]-Cu^{2+}). Thus, the use of the

Cutrz precursor is essential to produce catalytic active sites of r[Cutrz/GO].

Durability tests at pH 7 under O_2 unveiled that almost no activity loss was observed with low H_2O_2 production (<5%) even after 8000 potential cycles under oxygen (**Figure 2b**). These results indicate that r[Cutrz/GO] is robust in the copper-based ORR catalysts.[12,14,15] The carbon corrosion, which occurs at >1.0 V vs. RHE,[36] is excluded in our durability experiments. This high durability of r[Cutrz/GO] may originate from the stability of the copper reaction sites against dissolution and/or the high product selectivity to water.

Physicochemical measurements on r[Cutrz/GO] revealed the formation of sp^2 carbon networks after the heating treatment. The electrocatalyst r[Cutrz/GO] had an exfoliated sheet-like structure, confirmed by TEM images (**Figure S5**), with a Brunauer-Emmett-Teller (BET) specific surface area of 273 $m^2\ g^{-1}$ (**Figure S6**). A C1s XP spectrum of r[Cutrz/GO] exhibited the main peak for C=C at 284.7 eV, whereas two peaks were observed for C=C at 284.7 eV and for C–O at ca. 287 eV in an XP spectrum of the precursor mixture of Cutrz/GO (**Figure S7**), suggesting that oxygen functional groups were removed from GO during the pyrolysis, followed by the formation of sp^2 carbon networks.[19,20] A Raman spectrum of r[Cutrz/GO] showed the D-band at 1350 cm^{-1} and the G-band at 1580 cm^{-1}, assigned to edge or defect sites and to sp^2 carbon

sheets, respectively.[20] An intensity ratio of the D-band to the G-band was calculated to be 1.07, which was higher than the value of 0.93 for GO (**Figure S8**), implying that the incorporation of copper and nitrogen atoms in sp^2 carbon networks after the pyrolysis.[19] ICP-AES and elemental analysis of r[Cutrz/GO] gave copper and nitrogen contents to be 0.28 wt% and 1.06 wt%, respectively. The molar ratio of N to Cu was determined to be approximately 17:1.

The peak deconvolution analysis of N1s XP spectra suggests that r[Cutrz/GO] had mainly pyridinic nitrogen atoms. The peak deconvolution gave three components for r[Cutrz/GO]: 52% at 398.8 eV, 27% at 401.0 eV and 21% at 401.8 eV (**Figure S9b**), which were assigned to pyridinic, pyrrolic and quaternary nitrogen atoms, respectively.[37] For Cutrz, only two components were observed: 17% at 399.3 eV and 83% at 400.3 eV (**Figure S9a**). These components were assigned to imine nitrogen atoms in the triazole ring and/or to the nitrogen atoms of the deprotonated triazole ring.[38,39] The difference between r[Cutrz/GO] and Cutrz in N1s XP spectra suggests that some nitrogen atoms in the triazole ring were converted to pyridinic nitrogen atoms during the heat treatment. Since pyridinic and pyrrolic (or remaining triazole) nitrogen atoms have a lone pair of electrons, these nitrogen atoms in r[Cutrz/GO] may form coordination bonding with copper ions.

Multinuclear copper sites in nitrogen-doped graphene for r[Cutrz/GO] may be visualized by atomic resolution HAADF microscopy coupled with STEM (**Figure 3a**). The presence of copper ions was confirmed by EDS of r[Cutrz/GO] (**Figure S10**). XAS measurements at Cu L_3-edge suggest that r[Cutrz/GO] had copper ions with oxidation states of Cu^{II} as well as Cu^{I}. Two peaks at ca. 931 eV and 934 eV were observed for r[Cutrz/GO] (**Figure 3b**) and were assigned to Cu^{II} and Cu^{I} ions, respectively, because Cutrz that has Cu^{II} ions showed a peak at ca. 931 eV, and the peak at 934 eV was characteristic for Cu^{I} species.[40]

To obtain structural information on the copper sites under catalytic and non-catalytic conditions, potential dependent Cu *K*-edge XAS measurements of r[Cutrz/GO] were performed. A characteristic Cu^{I} shoulder peak[28] was observed at ca. 8983 eV at 0 V vs. RHE under O_2 (a catalytic condition) in the X-ray near edge structure (XANES) region (**Figure 3c**), implying that Cu^{I} sites may work as the active site for r[Cutrz/GO]. This XANES spectrum was clearly different from those recorded under non-catalytic conditions: at +1.0 V vs. RHE under N_2; +1.0 V vs. RHE under O_2; and 0 V vs. RHE under N_2 (**Figures S11** and **S12**). Thus, the reduction of Cu^{II} to Cu^{I} in the presence of oxygen may activate r[Cutrz/GO] for the ORR.

Ii is most likely that r[Cutrz/GO] has multinuclear copper sites and an unsaturated

coordination environment, suggested by Fourier transforms of EXAFS (FT-EXAFS) of r[Cutrz/GO]. FT-EXAFS patterns at +1.0 and 0 V vs. RHE under O_2 showed two peaks in the *R* range between 1.0 and 2.5 Å (**Figure 3d**). The curve-fitting analysis of these FT-EXAFS patterns gave coordination numbers of Cu−N to be 2.6±0.4 at +1.0 V and 2.3±0.5 at 0 V and coordination numbers of Cu···Cu to be 0.5±0.4 at +1.0 V and 1.4±0.1 at 0 V (**Table S2**). These results indicate that r[Cutrz/GO] has low Cu–N coordination numbers and multinuclear Cu active sites. Cu active sites with such low Cu–N coordination numbers may play an important role in oxygen binding.[14,41] The curve-fitting analysis also gave a Cu−N bond length of 1.87±0.02 Å and a Cu···Cu distance with 2.55±0.01 Å at 0 V under O_2 (**Table S2**). This Cu···Cu distance falls in a distribution of intramolecular Cu···Cu distances of multinuclear Cu^I complexes,[42] also suggesting the presence of multinuclear Cu^I active sites even under catalytic conditions. Note that EXAFS oscillations were clearly different between r[Cutrz/GO] (**Figure S13**), copper foil (**Figure S14**) and Cutrz (**Figure S15**), excluding the presence of neither Cutrz nor metallic copper in r[Cutrz/GO].

4. CONCLUSIONS

We incorporated multinuclear copper active sites with low Cu–N coordination numbers in nitrogen-doped graphene for the electrochemical ORR. The r[Cutrz/GO]

electrocatalyst showed high ORR catalytic activity and durability in Cu-based ORR electrocatalysts, thanks to the multinuclear active site. Our synthetic approach can, in principle, be applied to the incorporation of other multinuclear transition metal active sites in nitrogen-doped graphene and will open new possibilities to developing non-PGM-based electrocatalysts not only for the ORR but also other electrochemical reactions related to sustainable energy production, since multinuclear metal active sites are found in metalloenzymes such as hydrogenases and carbon monoxide dehydrogenases.[43]

ASSOCIATED CONTENT

Supporting Information. The Supporting Information is available free of charge on the ACS Publications website at DOI: XXX. Experimental section, XRD patterns, cyclic voltammograms, linear sweep voltammograms, TEM images, an N_2 adsorption/desorption isotherm, X-ray photoelectron spectra, Raman spectra, XANES data, EXAFS data and a list of abbreviations of the samples used (PDF).

AUTHOR INFORMATION

Corresponding Authors

*E-mail: masaru.kato@ees.hokudai.ac.jp

*E-mail: iyagi@ees.hokudai.ac.jp

Notes

The authors declare on competing financial interest.

ORCID

Masaru Kato: 0000-0002-2845-3525

Asakura Kiyotaka: 0000-0003-1077-5996

ACKNOWLEDGMENTS

The authors would like to thank Shingo Mukai, Yusuke Kawamura (Technical Division, Institute for Catalysis, Hokkaido University), Takao Ohta, Naomi Hirai, Yukiko Takahashi (Research Institute for Electronic Science, Hokkaido University) and Ryo Ota (Graduate School of Engineering, Hokkaido University) for their technical supports on experiments; Dr. Hiroyuki Asakura and Prof. Masao Tabuchi (Aichi Synchrotron Radiation Center, Nagoya University) for XAS measurements; and Ryota Kumagai, Dr. Satoshi Yasuda and Prof. Kei Murakoshi (Faculty of Science, Hokkaido University) for Raman spectroscopy measurements. This work was supported by a Program for Development of Environmental Technology using Nanotechnology from the MEXT, Japan; Nanotechnology Platform Programs of MEXT at Hokkaido University and JAEA; the Fusion-H program at Hokkaido University; and the project "Development of Advanced PEFC Utilization Technologies/Development of Fundamental Technologies

for PEFC Promotion/Highly-Coupled Analysis of Phenomena in MEA and its Constituents and Evaluation of Cell Performance" of NEDO, Japan. XAS experiments were performed at the beamlines BL12C and BL9C in Photon Factory (Proposal Nos. 2010G200, 2015G103, and 2016G671), at the JAEA beamline BL14B1 (Proposal Nos. 2016B3631 and 2017A3631) and the RIKEN beamline BL17SU (Proposal Nos. 20160069, 20170077 and 20170114) in SPring-8, and at the beamline BL5S1 in Aichi Synchrotron Radiation Center (Proposal No. 201504026).

References

(1) Banham, D.; Ye, S. Current Status and Future Development of Catalyst Materials and Catalyst Layers for Proton Exchange Membrane Fuel Cells: An Industrial Perspective. *ACS Energy Lett.* **2017**, *2*, 629–638.

(2) Li, Y.; Dai, H.; Chen, Y. H.; Bruce, P. G.; Hardwick, L. J.; Barde, F.; Novak, P.; Bruce, P. G.; Dai, H. J. Recent Advances in Zinc–air Batteries. *Chem. Soc. Rev.* **2014**, *43*, 5257–5275.

(3) Lefèvre, M.; Proietti, E.; Jaouen, F.; Dodelet, J.-P. Iron-Based Catalysts with Improved Oxygen Reduction Activity in Polymer Electrolyte Fuel Cells. *Science* **2009**, *324*, 71–74.

(4) Wu, G.; More, K. L.; Johnston, C. M.; Zelenay, P. High-Performance Electrocatalysts for Oxygen Reduction Derived from Polyaniline, Iron, and Cobalt. *Science* **2011**, *332*, 443–447.

(5) Nabae, Y.; Nagata, S.; Hayakawa, T.; Niwa, H.; Harada, Y.; Oshima, M.; Isoda, A.; Matsunaga, A.; Tanaka, K.; Aoki, T. Pt-Free Carbon-Based Fuel Cell Catalyst Prepared from Spherical Polyimide for Enhanced Oxygen Diffusion. *Sci. Rep.* **2016**, *6*, 23276.

(6) Sa, Y. J.; Seo, D.-J.; Woo, J.; Lim, J. T.; Cheon, J. Y.; Yang, S. Y.; Lee, J. M.;

Kang, D.; Shin, T. J.; Shin, H. S.; Jeong, H. Y.; Kim, C. S.; Kim, M. G.; Kim, T.-Y.; Joo, S. H. A General Approach to Preferential Formation of Active Fe–Nx Sites in Fe–N/C Electrocatalysts for Efficient Oxygen Reduction Reaction. *J. Am. Chem. Soc.* **2016**, *138*, 15046–15056.

(7) Armel, V.; Hindocha, S.; Salles, F.; Bennett, S.; Jones, D.; Jaouen, F. Structural Descriptors of Zeolitic–Imidazolate Frameworks Are Keys to the Activity of Fe–N–C Catalysts. *J. Am. Chem. Soc.* **2017**, *139*, 453–464.

(8) Chung, H. T.; Cullen, D. A.; Higgins, D.; Sneed, B. T.; Holby, E. F.; More, K. L.; Zelenay, P. Direct Atomic-Level Insight into the Active Sites of a High-Performance PGM-Free ORR Catalyst. *Science* **2017**, *357*, 479–484.

(9) Varnell, J. A.; Tse, E. C. M.; Schulz, C. E.; Fister, T. T.; Haasch, R. T.; Timoshenko, J.; Frenkel, A. I.; Gewirth, A. A. Identification of Carbon-Encapsulated Iron Nanoparticles as Active Species in Non-Precious Metal Oxygen Reduction Catalysts. *Nat. Commun.* **2016**, 12582.

(10) Zitolo, A.; Goellner, V.; Armel, V.; Sougrati, M.-T.; Mineva, T.; Stievano, L.; Fonda, E.; Jaouen, F. Identification of Catalytic Sites for Oxygen Reduction in Iron- and Nitrogen-Doped Graphene Materials. *Nat. Mater.* **2015**, *14*, 937–942.

(11) Mano, N.; Soukharev, V.; Heller, A. A Laccase-Wiring Redox Hydrogel for

Efficient Catalysis of O_2 Electroreduction. *J. Phys. Chem. B* **2006**, *110*, 11180–11187.

(12) Thorum, M. S.; Yadav, J.; Gewirth, A. A. Oxygen Reduction Activity of a Copper Complex of 3,5-Diamino-1,2,4-Triazole Supported on Carbon Black. *Angew. Chem. Int. Ed.* **2009**, *48*, 165–167.

(13) Wang, J.; Wang, K.; Wang, F. B.; Xia, X. H. Bioinspired Copper Catalyst Effective for Both Reduction and Evolution of Oxygen. *Nat. Commun.* **2014**, *5*, 5285.

(14) Iwase, K.; Yoshioka, T.; Nakanishi, S.; Hashimoto, K.; Kamiya, K. Copper-Modified Covalent Triazine Frameworks as Non-Noble-Metal Electrocatalysts for Oxygen Reduction. *Angew. Chem. Int. Ed.* **2015**, *54*, 11068–11072.

(15) Koshikawa, H.; Nakanishi, S.; Hashimoto, K.; Kamiya, K. Heat-Treated 3,5-Diamino-1,2,4-Triazole/graphene Hybrid Functions as an Oxygen Reduction Electrocatalyst with High Activity and Stability. *Electrochim. Acta* **2015**, *180*, 173–177.

(16) Xi, Y.-T.; Wei, P.-J.; Wang, R.-C.; Liu, J.-G. Bio-Inspired Multinuclear Copper Complexes Covalently Immobilized on Reduced Graphene Oxide as Efficient

Electrocatalysts for the Oxygen Reduction Reaction. *Chem. Commun.* **2015**, *51*, 7455–7458.

(17) Yamada, T.; Maruta, G.; Takeda, S. Reversible Solid-State Structural Conversion between a Three-Dimensional Network and a One-Dimensional Chain of Cu(II) Triazole Coordination Polymers in Acidic/basic-Suspensions or Vapors. *Chem. Commun.* **2011**, *47*, 653–655.

(18) Kato, M.; Oyaizu, N.; Shimazu, K.; Yagi, I. Oxygen Reduction Reaction Catalyzed by Self-Assembled Monolayers of Copper-Based Electrocatalysts on a Polycrystalline Gold Surface. *J. Phys. Chem. C* **2016**, *120*, 15814–15822.

(19) Kamiya, K.; Hashimoto, K.; Nakanishi, S. Instantaneous One-Pot Synthesis of Fe–N-Modified Graphene as an Efficient Electrocatalyst for the Oxygen Reduction Reaction in Acidic Solutions. *Chem. Commun.* **2012**, *48*, 10213–10215.

(20) Marcano, D. C.; Kosynkin, D. V; Berlin, J. M.; Sinitskii, A.; Sun, Z.; Slesarev, A.; Alemany, L. B.; Lu, W.; Tour, J. M. Improved Synthesis of Graphene Oxide. *ACS Nano* **2010**, *4*, 4806–4814.

(21) Hummers, W. S.; Offeman, R. E. Preparation of Graphitic Oxide. *J. Am. Chem. Soc.* **1958**, *80*, 1339–1339.

(22) Kato, M.; Murotani, T.; Yagi, I. Bioinspired Iron- and Copper-Incorporated Carbon Electrocatalysts for Oxygen Reduction Reaction. *Chem. Lett.* **2016**, *45*, 1213–1215.

(23) Zook, L. A.; Leddy, J. Density and Solubility of Nafion: Recast, Annealed, and Commercial Films. *Anal. Chem.* **1996**, *68*, 3793–3796.

(24) Oura, M.; Nakamura, T.; Takeuchi, T.; Senba, Y.; Ohashi, H.; Shirasawa, K.; Tanaka, T.; Takeuchi, M.; Furukawa, Y.; Hirono, T.; Ohata, T.; Kitamura, H.; Shin, S. Degree of Circular Polarization of Soft X-Rays Emitted from a Multi-Polarization-Mode Undulator Characterized by Means of Magnetic Circular Dichroism Measurements. *J. Synchrotron Radiat.* **2007**, *14*, 483–486.

(25) Ohashi, H.; Senba, Y.; Kishimoto, H.; Miura, T.; Ishiguro, E.; Takeuchi, T.; Oura, M.; Shirasawa, K.; Tanaka, T.; Takeuchi, M.; Takeshita, K.; Goto, S.; Takahashi, S.; Aoyagi, H.; Sano, M.; Furukawa, Y.; Ohata, T.; Matsushita, T.; Ishizawa, Y.; Taniguchi, S.; Asano, Y. Performance of a Highly Stabilized and High-Resolution Beamline BL17SU for Advanced Soft X-Ray Spectroscopy at SPring-8. In *AIP Conference Proceedings*; AIP, 2007; Vol. 879, pp 523–526.

(26) Tokushima, T.; Horikawa, Y.; Arai, H.; Harada, Y.; Takahashi, O.; Pettersson, L. G. M.; Nilsson, A.; Shin, S. Polarization Dependent Resonant X-Ray Emission

Spectroscopy of D_2O and H_2O Water: Assignment of the Local Molecular Orbital Symmetry. *J. Chem. Phys.* **2012**, *136*, 44517.

(27) Horikawa, Y.; Tokushima, T.; Hiraya, A.; Shin, S. Pronounced Polarization Anisotropy in Resonant X-Ray Emission from Acetic Acid Molecules in Solution. *Phys. Chem. Chem. Phys.* **2010**, *12*, 9165.

(28) Kato, M.; Kimijima, K.; Shibata, M.; Notsu, H.; Ogino, K.; Inokuma, K.; Ohta, N.; Uehara, H.; Uemura, Y.; Oyaizu, N.; Ohba, T.; Takakusagi, S.; Asakura, K.; Yagi, I. Deprotonation of a Dinuclear Copper Complex of 3,5-Diamino-1,2,4-Triazole for High Oxygen Reduction Activity. *Phys. Chem. Chem. Phys.* **2015**, *17*, 8638–8641.

(29) Zabinsky, S. I.; Rehr, J. J.; Ankudinov, A.; Albers, R. C.; Eller, M. J. Multiple-Scattering Calculations of X-Ray-Absorption Spectra. *Phys. Rev. B* **1995**, *52*, 2995–3009.

(30) Rehr, J. J.; Albers, R. C. Theoretical Approaches to X-Ray Absorption Fine Structure. *Rev. Mod. Phys.* **2000**, *72*, 621–654.

(31) Ouellette, W.; Prosvirin, A. V.; Chieffo, V.; Dunbar, K. R.; Bruce Hudson, A.; Zubieta, J. Solid-State Coordination Chemistry of the Cu/Triazolate/X System (X = F^-, Cl^-, Br^-, I^-, OH^-, and SO_4^{2-}). **2006**, *45*, 9346–9366.

(32) Taguchi, T.; Takeyoshi. REX2000 Version 2.5: Improved DATA Handling and Enhanced User-Interface. In *AIP Conference Proceedings*; AIP, 2007; Vol. 882, pp 162–164.

(33) Taguchi, T.; Ozawa, T.; Yashiro, H. REX2000 Yet Another XAFS Analysis Package. *Phys. Scr.* **2005**, *2005*, 205.

(34) Asakura, K. Analysis of XAFS. In *X-Ray Absorption Fine Structure for Catalysts and Surfaces*; Iwasawa, Y., Ed.; Series on Synchrotron Radiation Techniques and Applications; WORLD SCIENTIFIC: Singapore, 1996; pp 33–58.

(35) Wang, F.-F.; Zhao, Y.-M.; Wei, P.-J.; Zhang, Q.-L.; Liu, J.-G. Efficient Electrocatalytic O_2 Reduction at Copper Complexes Grafted onto Polyvinylimidazole Coated Carbon Nanotubes. *Chem. Commun.* **2017**, *53*, 1514–1517.

(36) Banham, D.; Ye, S.; Pei, K.; Ozaki, J.; Kishimoto, T.; Imashiro, Y. A Review of the Stability and Durability of Non-Precious Metal Catalysts for the Oxygen Reduction Reaction in Proton Exchange Membrane Fuel Cells. *J. Power Sources* **2015**, *285*, 334–348.

(37) Matter, P. H.; Zhang, L.; Ozkan, U. S. The Role of Nanostructure in Nitrogen-Containing Carbon Catalysts for the Oxygen Reduction Reaction. *J.*

Catal. **2006**, *239*, 83–96.

(38) Babić-Samardžija, K.; Lupu, C.; Hackerman, N.; Barron, A. R.; Luttge, A. Inhibitive Properties and Surface Morphology of a Group of Heterocyclic Diazoles as Inhibitors for Acidic Iron Corrosion. *Langmuir* **2005**, *21*, 12187–12196.

(39) Wrzosek, B.; Bukowska, J. Molecular Structure of 3-Amino-5-Mercapto-1, 2, 4-Triazole Self-Assembled Monolayers on Ag and Au Surfaces. *J. Phys. Chem. C* **2007**, *111*, 17397–17403.

(40) Grioni, M.; van Acker, J. F.; Czyžyk, M. T.; Fuggle, J. C. Unoccupied Electronic Structure and Core-Hole Effects in the X-Ray-Absorption Spectra of Cu_2O. *Phys. Rev. B* **1992**, *45*, 3309–3318.

(41) Wu, H.; Li, H.; Zhao, X.; Liu, Q.; Wang, J.; Xiao, J.; Xie, S.; Si, R.; Yang, F.; Miao, S.; Guo, S.; Wang, G.; Bao, X. Highly Doped and Exposed Cu(i)–N Active Sites within Graphene towards Efficient Oxygen Reduction for Zinc–air Batteries. *Energy Environ. Sci.* **2016**, *9*, 3736–3745.

(42) Carvajal, M. A.; Alvarez, S.; Novoa, J. J. The Nature of Intermolecular $Cu^{I}\cdots Cu^{I}$ Interactions: A Combined Theoretical and Structural Database Analysis. *Chem. Eur. J.* **2004**, *10*, 2117–2132.

(43) Armstrong, F. A.; Hirst, J. Reversibility and Efficiency in Electrocatalytic Energy Conversion and Lessons from Enzymes. *Proc. Natl. Acad. Sci.* **2011**, *108*, 14049–14054.

Figure captions

Figure 1. Schematic representation of the synthetic procedure of r[Cutrz/GO].

Figure 2. (a) LSVs of r[Cutrz/GO] and five control samples: GO-supported Cutrz (Cutrz/GO); the Cu-doped (N-free) graphene (r[Cu/GO]); the rGO-supported Cutrz (Cutrz/rGO); the N-doped (Cu-free) graphene (r[trz/GO]); and the r[trz/GO] that was treated with an aqueous solution containing Cu^{2+} (r[trz/GO]-Cu^{2+}). These abbreviations are listed in Table S1. (b) LSVs of of r[Cutrz/GO] before (in gray) and after (in black) 8000 potential cycles (b') with the corresponding ring currents. A bias potential of +1.2 V vs. RHE was applied to the ring electrode. The potential cycles were performed at 100 mV s^{-1} in the potential range between +0.50 and +0.90 V vs. RHE under O_2. All LSVs in (a) and (b) were recorded using a rotating ring disk electrode at 1600 rpm in the negative-going sweep at 5 mV s^{-1} in 0.04 M Britton-Robinson buffered solution containing 0.1 M $NaClO_4$ at pH 7 under O_2.

Figure 3. (a) A representative STEM-HAADF image of r[Cutrz/GO]. (b) Cu L_3-edge X-ray absorption spectra of Cu plate, r[Cutrz/GO] and Cutrz. (c) Potential dependent Cu *K* edge XANES spectra of r[Cutrz/GO] recorded in the 0.04 M Britton-Robinson buffered aqueous solution containing 0.1 M $NaClO_4$ at pH 7 at +1.0 V (in gray) and at 0 V vs. RHE (in black) under oxygen. (d) FT-EXAFS of r[Cutrz/GO] at +1.0 V (in gray)

and at 0 V vs. RHE (in black).

Figures

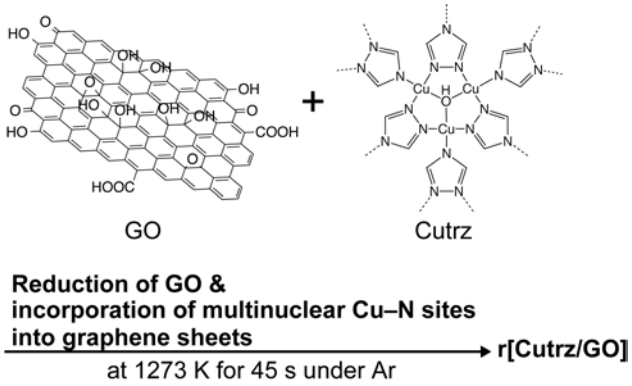

Figure 1

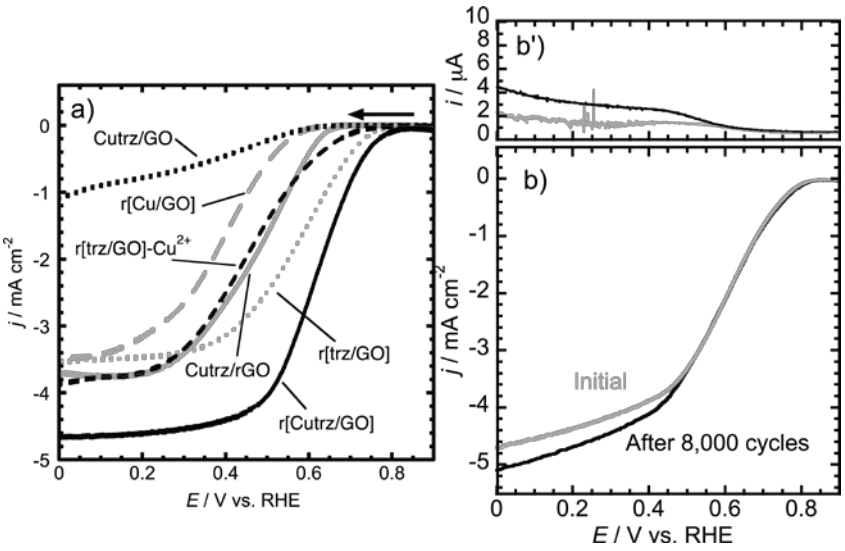
a)
Cutrz/GO
r[Cu/GO]
r[trz/GO]-Cu2+
Cutrz/rGO
r[trz/GO]
r[Cutrz/GO]
j / mA cm-2
E / V vs. RHE
b')
i / µA
b)
Initial
After 8,000 cycles
j / mA cm-2
E / V vs. RHE

Figure 2

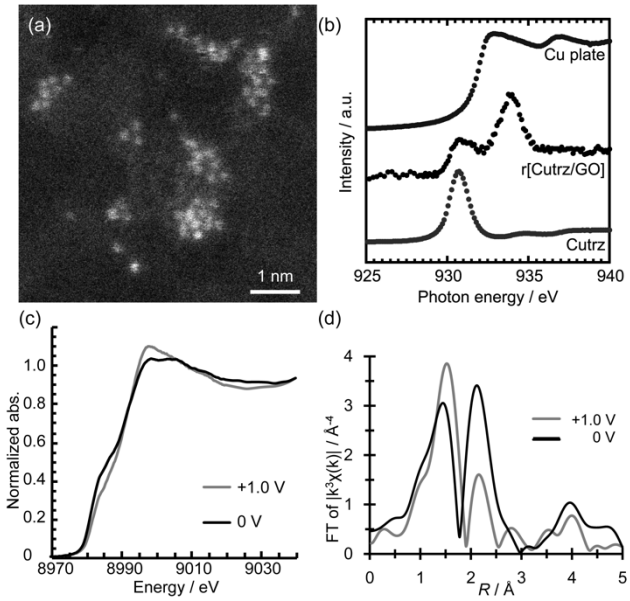
(a)
1 nm
(b)
Cu plate
r[Cutrz/GO]
Cutrz
Intensity / a.u.
925
930
935
940
Photon energy / eV
(c)
Normalized abs.
1.0
0.8
0.6
0.4
0.2
0
+1.0 V
0 V
8970
8990
9010
9030
Energy / eV
(d)
FT of |k³χ(k)| / Å⁻⁴
4
3
2
1
0
+1.0 V
0 V
0
1
2
3
4
5
R / Å

Figure 3

TOC graphic.